Journal of Energy and Power Engineering 8 (2014) 1964-1973

Calculation of Steady SF_6 Gas Flow through a 420 kV Circuit Breaker Nozzle and Electric Field Distribution

Dejan Bešlija[1, 2], Sead Delić[1, 2], Kyong-Hoe Kim [1, 3], Mirsad Kapetanović[1, 2] and Almir Ahmethodžić[1]

1. Faculty of Electrical Engineering, University of Sarajevo, Sarajevo 71000, Bosnia and Herzegovina

2. EnergoBos ILJIN d. o. o., Sarajevo 71000, Bosnia and Herzegovina

3. ILJIN Electric Co. Ltd., Seoul 121-716, Republic of Korea

Received: July 17, 2014 / Accepted: September 01, 2014 / Published: November 30, 2014.

Abstract: Special interest in current interruptions is dedicated to the processes close to the current zero instant, the so-called interaction region, which determines the circuit breakers' performance. The quantities of interest in this region are the distribution of temperature, density and pressure, velocity and gas mass flow along the electric arc axis, as well as the distribution of electric stress between contacts. Calculation of steady SF_6 gas flow through the nozzle of a 420 kV circuit breaker at the current zero instant, for different arcing durations, was carried out using a commercial CFD (computational fluid dynamics) simulation tool. The calculation results were used to get insight into improvement possibilities of the SF_6 gas flow model used in the software for computer simulation of HV (high-voltage) circuit breakers. Electric field calculation results were performed for the same 420 kV circuit breaker, in order to estimate the breakdown voltage at the current zero instant.

Key words: HV SF_6 circuit breaker, nozzle, gas flow regime, shock wave, breakdown voltage.

1. Introduction

A serious approach to design of switching devices requires a basic knowledge of physical processes related to the electric arc, arc establishing and characteristics. The question of electric arc instability is crucial, not only for switching devices, but also for many other devices where it is used as the key phenomena, e.g., arc furnaces, arc welding, etc.. In these cases, maintaining of arc stability is important, while for switching devices, this is not the case. For switching devices, quite opposite conditions are desirable, i.e., unstable arc burning [1].

For AC (alternating current) switching, special interest is devoted to processes that happen at and around the moment when the current passes through its zero. This time interval, about 100 μs before and after current zero, is called the interaction interval. The interaction interval is the time from the start of significant change in arc voltage, prior to current zero, to the moment when the current, including the post-arc current, if any, ceases to flow. During the interaction interval, the short circuit current stress changes into high voltage stress, and the circuit breaker behavior significantly influences the current and the voltages in the circuit. This interaction between the circuit and the circuit breaker during the interaction interval is of extreme importance to the interrupting process and determines its breaking performance. The distribution of following variables in the interaction region is of high importance: SF_6 gas pressure and density, gas velocity along the electric arc axis, as well as electric stress in the contact gap [2].

A proper design of circuit breaker components is of high importance for its breaking capability and the dielectric recovery of the contact gap (more intensive evacuation of hot gases), since the gas flow is highly dependent on the nozzle downstream shape. Interaction

Corresponding author: Dejan Bešlija, Ph.D. student, research field: development of HV circuit breakers. E-mail: dejan.beslija@gmail.com.

of the gas flow and the electric field creates critical regions characterized by low gas density and high electric field strength. The probability of dielectric breakdown in these regions is very high. Therefore, for the given distribution of electric stresses in the contact gap, it is desirable to preserve the highest possible gas flow density. Since the local properties of gas flow determine its dielectric strength, it is very important to understand the dynamic flow behavior of gas through HV (high-voltage) SF_6 circuit breaker nozzles. CFD (computational fluid dynamics) offers big advantages regarding this matter, i.e., simulation and visualization of flow processes in HV circuit breakers. CFD analyses can save a large number of expensive testing shifts in HV power laboratories and significantly accelerate the prototype design process, which is directly related with the reduction of development expenses. Since the design methodology of HV circuit breakers is based primarily on experience and previous test results, it is necessary to invest great effort into developing such computer simulation tools, with the final goal to improve the performance of such apparatus.

2. Mathematical Model of Compressible Viscous Fluid Flow

Due to the compressible nature of SF_6 gas, the type of flow occurring during a HV circuit breaker opening operation is compressible. Having this in mind, the used mathematical model must take into account all possible compressibility effects. On the other hand, high flow velocities through HV circuit breaker nozzles dictate high Reynolds numbers. Therefore, viscous effects and turbulent flow behavior must also be taken into consideration. Accordingly, the flow type inside the analyzed HV circuit breaker is chosen to be compressible, viscous and turbulent, and includes equations for conservation of mass (continuity equation), momentum (Navier-Stokes equation), energy, turbulent kinetic energy and its dissipation, given in Eqs. (1)-(8), respectively [3]:

$$\frac{\partial \rho}{\partial t} + \nabla \cdot (\rho \vec{v}) = 0 \tag{1}$$

$$\rho\left(\frac{\partial \vec{v}}{\partial t} + (\vec{v} \cdot \nabla)\vec{v}\right) = -\nabla p + \nabla(\mu_e \nabla \cdot \vec{v}) + \frac{\mu_e}{3}\nabla(\nabla \cdot \vec{v}) \tag{2}$$

$$\frac{\partial}{\partial t}\left(\rho C_p T_0\right) + \left(\rho \vec{v} C_p T_0\right) = \nabla \cdot (\lambda_e \cdot \nabla T_0) + \frac{\partial p}{\partial t} + E^k + \theta + W^v \tag{3}$$

$$\frac{\partial \rho k}{\partial t} + \nabla \cdot (\rho k \vec{v}) = \nabla \cdot \left(\frac{\mu_t}{\sigma_k}\nabla k\right) + \mu_t \theta - \rho\varepsilon \tag{4}$$

$$\frac{\partial \rho \varepsilon}{\partial t} + \nabla \cdot (\rho \varepsilon \vec{v}) = \nabla \cdot \left(\frac{\mu_t}{\sigma_\varepsilon}\nabla \varepsilon\right) + C_{1\varepsilon}\mu_t \frac{\varepsilon}{k}\theta - C_{2\varepsilon}\rho\frac{\varepsilon^2}{k} \tag{5}$$

Wherein,

$$T_0 = T - \frac{v^2}{2C_p} \tag{6}$$

$$\mu_e = \mu_l + \mu_t = \mu_l + C_\mu \rho \frac{\varepsilon^2}{k} \tag{7}$$

$$\lambda_e = \lambda_l + \lambda_t = \lambda_l + \frac{\mu_t}{\sigma_\varepsilon} C_p \tag{8}$$

where, t is time, $\vec{v}, v$ are the velocity vector and its magnitude, ρ is gas density, p is static gas pressure, T_0 is total (stagnation) temperature, T is static temperature, C_p is specific heat capacity at constant pressure, μ_e is effective dynamic viscosity, μ_t is turbulent dynamic viscosity, μ_l is laminar dynamic viscosity, λ_e is effective thermal conductivity, λ_t is turbulent thermal conductivity, λ_l is laminar thermal conductivity, E^k is the kinetic energy term, θ is the viscous dissipation term, W^v is the viscous work term, k is turbulent kinetic energy, ε is the turbulent kinetic energy dissipation rate, σ_k is the turbulent Prandtl number for turbulent kinetic energy, σ_ε is the turbulent Prandtl number for dissipation of turbulent kinetic energy, σ_t is the energy Prandtl number, while C_μ, $C_{1\varepsilon}$, $C_{2\varepsilon}$ are the standard k-ε turbulence model coefficients. The model of SF_6 gas must completely reproduce the behavior of real SF_6 gas and have a sufficient temperature range of applicability.

In this range, it is necessary to provide lowest possible deviation of all gas parameters from their real values, and have appropriately modeled all required EOS (equations of state), needed to complete the gas flow model. They determine the following relationships:

$$\rho = f(p, T) \tag{9}$$

$$\mu_l = f(p, T) \tag{10}$$

$$\lambda_l = f(p, T) \tag{11}$$

$$C_p = f(p, T) \tag{12}$$

It is important to mention that the same SF_6 model [4] was used in all performed calculations (including CFD). Since the complete history of the interrupting process is responsible for arc behavior, the computer simulation must take into consideration the interrupting process from its very beginning.

A SF_6 circuit breaker is generally of cylindrical shape and with an existing axial symmetry, which allows a 2D flow simulation and can significantly reduce the necessary CPU (central processing unit) time duration. Also, for high pressure and temperature acting inside the circuit breaker, it is reasonable to assume local chemical, as well as local thermal equilibrium [5]. All performed calculation examples take into account the aforementioned, considering that the entire process up to the current zero is calculated using a high-voltage circuit breaker computer simulation tool [6].

Data obtained from this application represent input data for further calculations in a commercial CFD simulation tool. Amongst them are the following variables:

- position of arcing contacts inside the nozzle at current zero d_z (depending on arc duration t_a, contact penetration d_{pen} and their travel h);
- static pressure P, temperature T and density ρ at the inlet and outlet (s);
- total SF_6 gas mass flow at the inlet G_{inlet};
- individual gas mass flow at the outlet (s) G_{outlet};
- specific heat at constant pressure C_p at the inlet and outlet (s);
- specific heat at constant volume C_v at the inlet and outlet (s);
- speed of sound c at the inlet and outlet (s).

This is illustrated on the example of a simple one-sided exhaust nozzle (see Fig. 1).

The values of all aforementioned variables, which represent boundary conditions for steady flow CFD calculations, relate to the current zero instant, where the electric arc finally extinguishes. Variables of state of gas (pressure, temperature, specific density) are considered to be averaged values of those parameters. According to this assumption, variables of state of gas are describing the state of gas in the entire chamber volume. This will be of importance for defining of nozzle geometry, in the sense of prolonging the calculation domain to the surrounding circuit breaker chambers, especially for the thermal chamber, since the pressure rise in this chamber is the main cause for gas flow through the nozzle.

Input data in this form is not compatible with the input required for CFD boundary conditions. Therefore, it is necessary to adapt them, in order to meet the required input. Given below is a set of equations used for this purpose. This set is applied for every boundary of the calculation domain.

Eqs. (13) and (14) are used for establishing the total temperature T_0 and total pressure p_0 of the nozzle inlet boundary:

$$\frac{T_0}{T} = 1 + \frac{\kappa - 1}{2} M^2 \tag{13}$$

$$\frac{p_0}{p} = \left(1 + \frac{\kappa - 1}{2} M^2\right)^{\frac{\kappa}{\kappa - 1}} \tag{14}$$

where, κ is the isentropic expansion factor (ratio of the

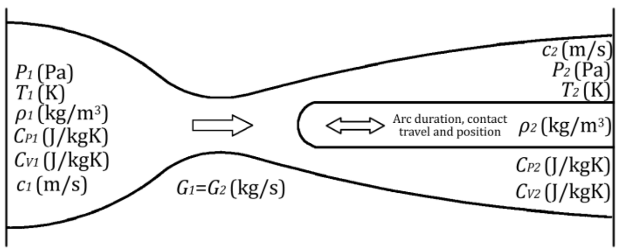

Fig. 1 One-Sided exhaust nozzle and necessary data obtained from the HV circuit breaker simulation tool [6].

specific heat capacity at constant pressure C_p to specific heat at constant volume C_v) and M is the Mach number (ratio of fluid speed v and speed of sound c):

$$\kappa = \frac{C_p}{C_v} \tag{15}$$

$$M = \frac{v}{c} \tag{16}$$

$$v = G \cdot \frac{1}{\rho} \cdot \frac{1}{A} \tag{17}$$

wherein, G is gas mass flow and A is the considered cross-sectional area. Eqs. (13)-(17) describe the variation of static pressure and temperature depending on flow velocity change (Mach number) with the assumption of an isentropic process. For a specific value of this ratio, for SF_6 gas, Eq. (13) predicts nozzle flow choking (M = 1, sonic flow) in the minimal cross-section, e.g., nozzle throat. In the cross-sectional area after the minimal, the gas can additionally accelerate, thus, establish supersonic flow conditions, characterized by a drop in pressure and gas density, which is most often the case in circuit breaker nozzles. If the supersonic flow is imposed to a pressure increase on the inlet boundary, a shock wave occurs, alongside with a sudden pressure drop. After the shock wave front, a subsonic region forms, where again, a gas density and pressure rise can be observed.

Further on, for determining of laminar dynamic viscosity, the Reynolds number Re and the turbulence intensity I [7], i.e., defining turbulence parameters at the boundaries, Eqs. (18)-(20) are used respectively:

$$\mu_l = 1.533 \cdot 10^{-5} + 4.8 \cdot 10^{-8} \cdot (T - 300) \tag{18}$$

$$Re = \frac{\rho D_H v}{\mu_l} \tag{19}$$

$$I = 0.16 \cdot Re_{D_H}^{-\frac{1}{8}} \tag{20}$$

Eqs. (19) and (20) introduce the so-called hydraulic diameter D_H of the circuit breaker nozzle inlet and outlet. This diameter for a cylindrical boundary is identical to its diameter, while for a coaxial cylindrical boundary with its inner and outer diameter, equals their difference [8].

3. Steady SF_6 Gas Flow through a 420 kV Circuit Breaker Nozzle

Test duty L75, according to IEC (International Electrotechnical Commission), for three different arcing times, 10, 15 and 20 ms (milliseconds), was analyzed in this paper. Thus, three CFD calculations of steady SF_6 gas flow through the analyzed 420 kV 63 kA circuit breaker were performed. The required geometry input and boundary conditions (see Table 1A in Appendix) for the current zero instant were obtained using the HV CB simulation tool. Results of these calculations are presented in Figs. 2 and 3. Depicted in these figures are the distribution of static pressure and the Mach number, and the distribution of density and gas velocity along the analyzed 420 kV circuit breaker nozzle for different arcing times, respectively. The drop of pressure in the downstream of the main and auxiliary nozzle indicates the appearance of a shock wave and a supersonic flow region in these locations.

The drop of pressure in the downstream of the main and auxiliary nozzle indicates the appearance of a shock wave and a supersonic flow region in these locations. This fact confirms also the distribution of Mach number in the nozzle downstreams. Nevertheless, the pressure ratios are not sufficient to expand the supersonic flow regions around the arcing contacts, associated with highly increased electric stresses. It can also be noticed that both auxiliary and main nozzles are chocked. The Mach number in both nozzles is equal to one, which means that the pressure ratios in both flow directions are sufficient in this case to cause their choking. The limitation of gas mass flow is due to the above described phenomenon. Therefore, gas mass flow limitation is defined by the minimal cross-sectional flow area and the established state of gas in this flow region. Most often, this happens inside the nozzle throat of the circuit breaker. If the pressure ratio is greater, the supersonic region expands even more into the nozzle downstream, i.e., the shock wave front dislocates further to the nozzle outlet. This applies to both main and auxiliary nozzles. For the minimal

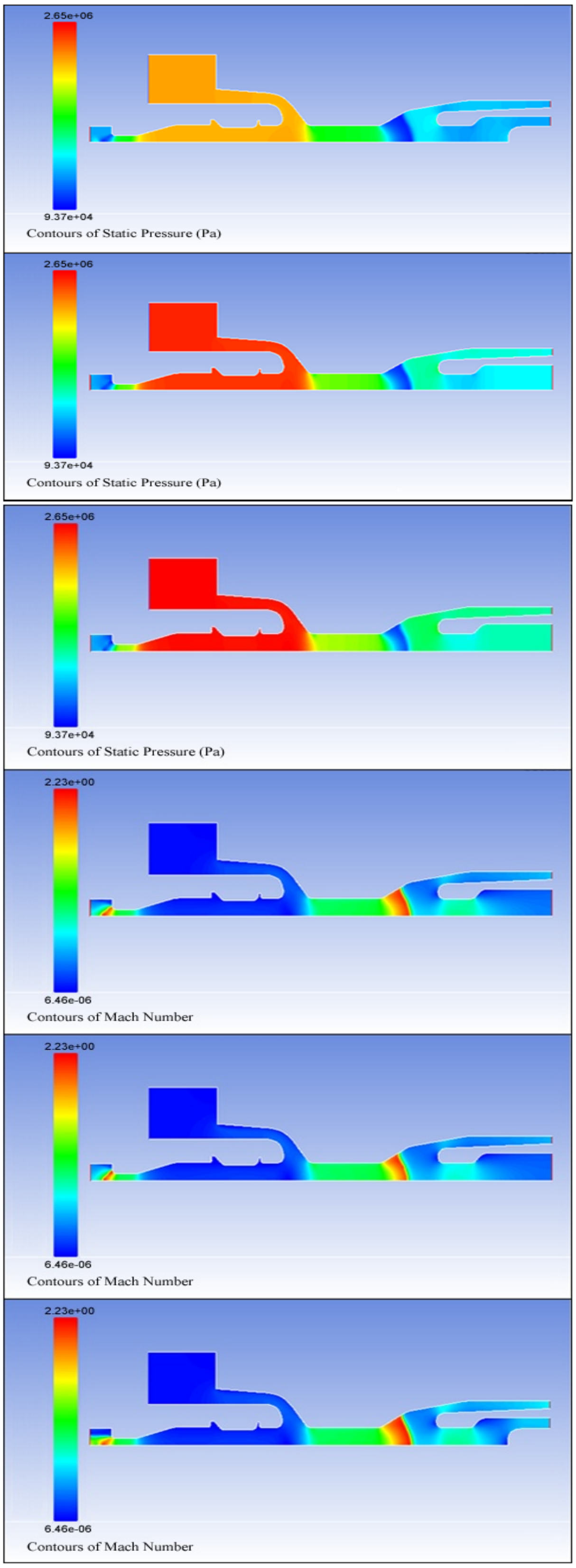

Fig. 2 Distribution of static pressure and Mach number along the 420 kV circuit breaker nozzle for different arcing durations.

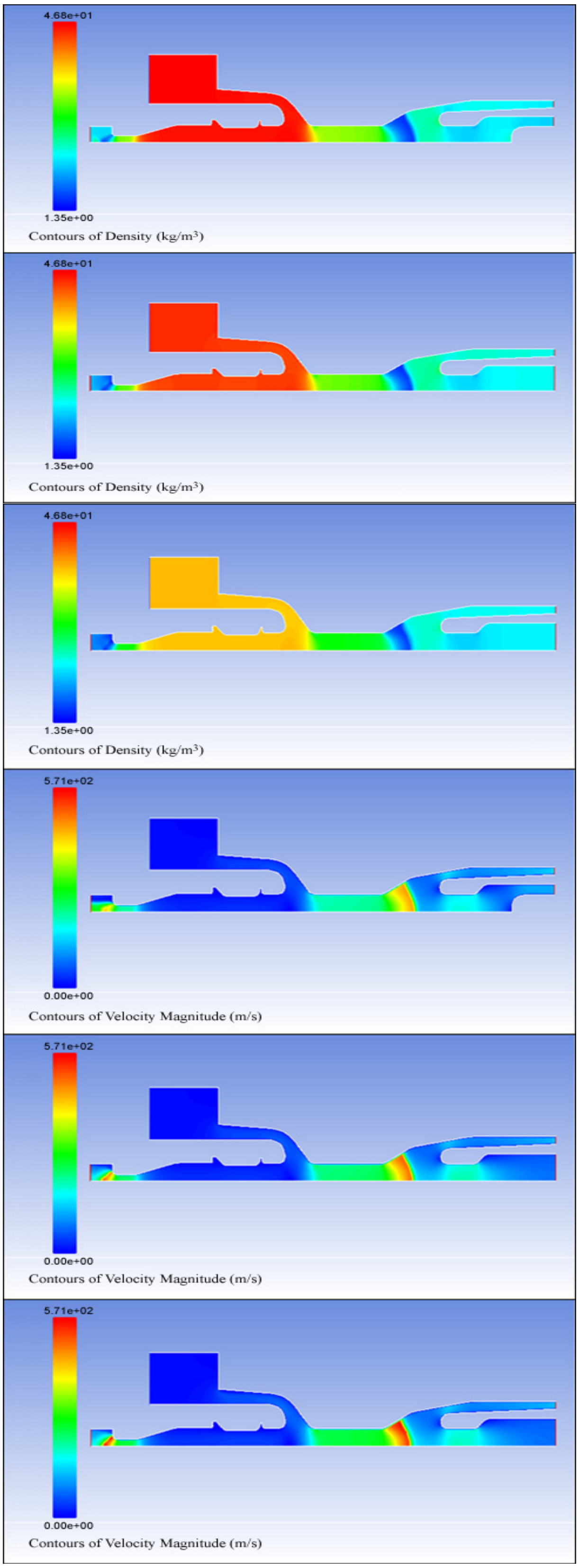

Fig. 3 Distribution of density and gas velocity along the 420 kV circuit breaker nozzle for different arcing durations.

arcing time of 10 ms, the main nozzle outlet pressure is the lowest of all analyzed, so that the shock wave front in this case is the farthest from the main nozzle throat. Since the main nozzle outlet pressure rises for longer arcing durations, the shock wave front retrieves ever more towards the main nozzle throat. Consequently, the supersonic region gets narrower. The pressure ratio in case of the auxiliary nozzle is largest for maximum, then medium and shortest arc duration, respectively (see Table 1A in Appendix). Table 2A (in Appendix) gives an overview of gas mass flow values calculated in CFD and the HV CB simulation tool. CFD calculations predict a lower value of gas mass flow at the current zero instant. This can be explained by Eq. (17) written in the following form:

$$G = v \cdot \rho \cdot A \tag{21}$$

Gas mass flow, according to Eq. (21), is defined by gas density and velocity, as well as the nozzle throat cross-sectional area. Since nozzle throats of both main and auxiliary nozzles of the analyzed 420 kV circuit breaker are choked at the current zero instant, the Mach number appearing in both throats is equal to one and sonic flow regime, i.e., gas speed equals the speed of sound of SF_6 gas. The calculated value of speed of sound in both used applications is the same; since they used the same SF6 gas model under the assumption of a isentropic process (speed of sound dominantly depends on gas temperature, which is approximately the same in both applications). Due to the use of a viscous flow model in the performed CFD calculations, the effective cross-sectional area is reduced due to friction on the nozzle walls and the characteristic near-wall velocity profile is obtained. This phenomenon is one of the reasons for lower values of gas mass flow in CFD compared to the ones obtained using the HV CB simulation tool. The second reason is lower gas density in the nozzle throat compared to the thermal chamber. Namely, in the HV CB simulation tool, it is assumed that state of gas in the nozzle throat equals the one in the thermal chamber, thus, not taking into account the reduction of gas density in the nozzle throat due to gas flow. This assumption additionally increases the gas mass flow.

On the other hand, by comparing the values of gas mass flow in Table 2A (in Appendix), it is important to notice that the mutual difference between ratios of gas mass which flows through the main and auxiliary nozzle compared to the total gas mass flow, for all arc durations, is less than 5%, and that only the values of gas mass flow show deviation due to previously discussed reasons. All gas mass flow reducing phenomena cannot be taken into account in the HV CB simulation tool.

The occurrence of shock waves is happening in the nozzle downstream, which is of high importance because it is very likely to coincide with high electrically stressed regions around the arcing contact tip. This coincidence of shock wave related gas density drop and high values of electric field strength is an undesirable phenomenon that should be avoided as much as possible.

The previous short analysis of some calculation results shows that CFD analyses represent a powerful tool for designing of HV circuit breaker nozzles and greatly helps in understanding of complex processes that happen inside SF_6 gas filled HV circuit breakers.

4. Electric Stresses of a 420 kV Circuit Breaker

Estimation of breakdown withstand voltage in high-voltage circuit breakers is a very challenging and demanding engineering problem. The breakdown withstand voltage U_p is estimated based on a criterion of dielectric strength of SF_6 gas, which is determined by the local gas flow field and the electric field distribution.

$$U_p = \mathrm{C} \cdot \left[\frac{\rho}{\hat{E}}\right]_{\min} \tag{22}$$

where, $\hat{E}$ is the local electric field strength when a unit voltage is applied. Constant C contains information about influences from surface roughness, area and voltage frequency on breakdown voltage. Measurements from cold dielectric experiments determine the contents of C. For a reliable estimation of breakdown withstand voltage, it is required to know the local density distribution (see Fig. 3), as well as the electric field distribution for the given nozzle geometry (see Fig.4). Fig. 5 depicts the chosen profile along which the breakdown voltage estimation will be performed. Results of this calculation are given in Fig. 6. The upper part of Fig. 6 shows the calculated electric field distribution, while the lower part depicts gas density along the same profile. The ratio of gas density and electric field strength in Eq. (22) multiplied by constant C, where C = 0.225 $(MVm)^2/kg$ is represented in Fig. 7.

The profile to be analyzed was not chosen randomly. It was selected to take into consideration high electric field strength around the arcing contacts, as well as the shock wave region in the nozzle downstream. The upper part of Fig. 6 indicates that the electric field strength peaks around the arcing contacts, while the lower part

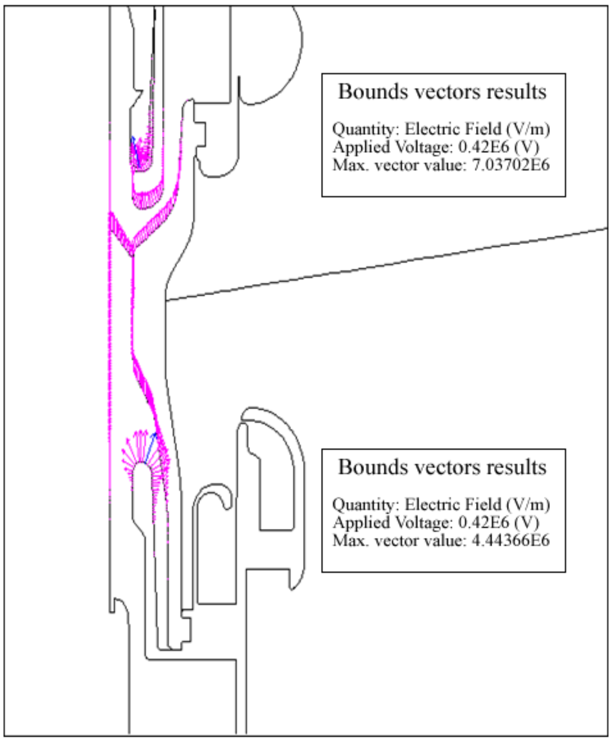

Fig. 4 Electric field strength vectors along the calculation domain boundary at minimum arcing duration inside the analyzed 420 kV circuit breaker.

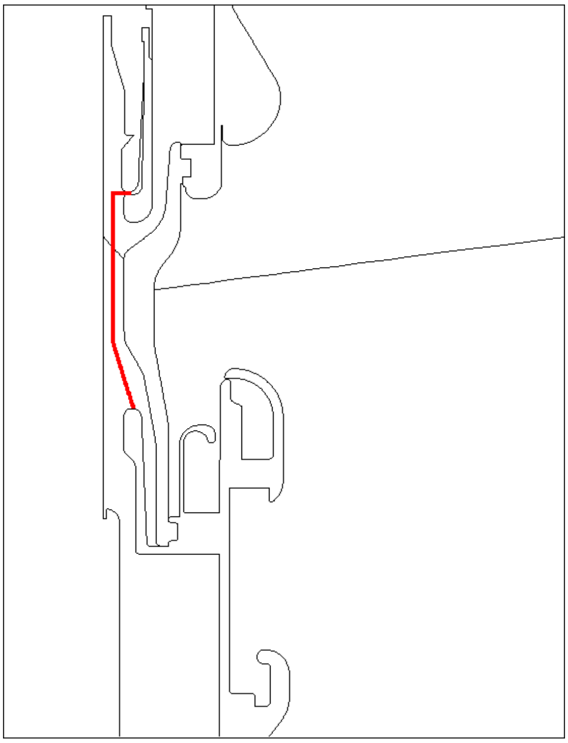

Fig. 5 Chosen profile for breakdown voltage estimation.

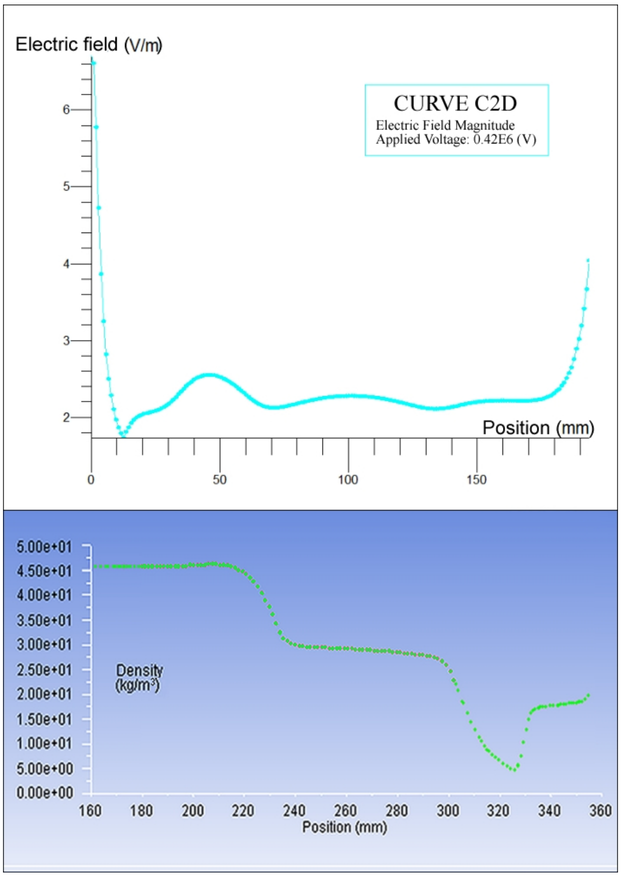

Fig. 6 Distribution of local electric field and gas density along the chosen estimation profile.

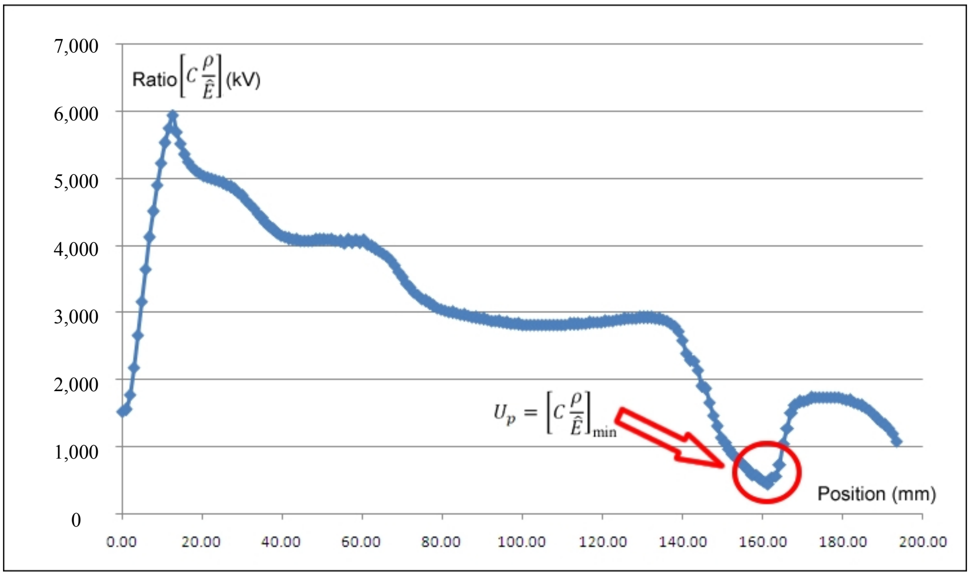

Fig. 7 Ratio of gas density and electric field strength along the chosen estimation profile.

of the same figure shows a pronounced gas density drop in the nozzle downstream where a shock wave occurs. Based on Eq. (22) and these two curves, the breakdown voltage along the chosen profile can be estimated (see Fig. 7). In the initial part of the breakdown voltage estimation curve along the chosen profile, it can be observed that the ratio of gas density and the local electric field strength dominantly follows the electric field strength curve, since gas density in this part of the nozzle is relatively constant. The local minimum of this ratio in this part of the chosen profile is located next to the arcing contact, due to the highest electric field strength at this place.

As distance from the arcing contact increases, the electric field strength decreases, so that the gas density and electric field strength ratio decreases. In the second part of the breakdown voltage curve along the chosen profile, the dominant influence on this ratio has gas density. This part of the profile passes through the supersonic region, which is characterized by high speeds and low gas densities. It can be noticed that the minimum value of the ratio of gas density and electric field strength is obtained in this region, which, according to Eq. (22), determines the breakdown withstand voltage. In the third part of the analyzed curve, there is an increase of gas density, while the electric field strength increases again, since this part of the chosen profile lies in the vicinity of the second arcing contact. Due to this increase, the ratio of gas density and electric field strength is decreasing. Thus, a considerable decrease of the analyzed ratio, whose minimum value defines the breakdown voltage, can be expected in regions with high electric field strengths (vicinity of arcing contacts) or in low-density regions (supersonic shock wave flow regions). For the analyzed case and chosen profile, the minimal ratio is located in the supersonic region.

6. Conclusions

This paper demonstrates a method for combining two computer applications using a system of Eqs. (13)-(20), which are used for adapting of certain output variables from one software, in this case, a fast and simple HV CB simulation tool, to the required input for more complex analyses in a CFD tool.

The model of SF_6 gas in calculations must accurately reproduce the behavior of real SF_6 gas, have a sufficiently wide temperature range of applicability in which lowest possible deviation of gas parameters from real values must be provided and have properly modeled all important characteristics. In this paper, such a model of real SF_6 gas was implemented. This model has a wide temperature range, which is very important for modeling of processes inside high-voltage circuit breakers, where gas temperatures can occur much over 1,000 K, due to large currents to be interrupted, and also modeled transport coefficients of thermal conductivity and SF_6 gas viscosity. They entail all viscous flow effects, such as flow separation, recirculation phenomena, backflow, near-wall effects, as well as turbulent behavior of gas, etc..

Steady flow calculations through a real-world 420 kV circuit breaker nozzle for different arcing durations confirm turbulent, viscous and compressible behavior of SF_6 gas, typical for convergent-divergent nozzles, as used in HV circuit breakers.

The analysis conducted in this paper can give guidelines for improvement possibilities of the HV CB simulation tool which is reflected in the limitation of the evidently increased gas mass flow by calculating the state of gas in the nozzle throat in every time step, as well as the implementation of viscous SF_6 gas behavior that would also introduce gas mass flow limitation effects. Another challenging task would be improvement of this simulation tool by introducing a proper shock wave and supersonic flow model.

Calculations of this type may further on be used as the basis for additional analyses regarding processes in HV circuit breakers. This possibility is demonstrated in this paper in the form of a breakdown voltage estimation analysis that can be used for small capacitive current switching duties or heavy current interruption duties after current zero [3]. Results of the performed estimation show that a substantial decrease of the ratio of gas density and the electric field strength in the nozzle downstream can be expected, due to a significant drop in gas density at this region.

Finally, it can be said that the analyses performed throughout this work represent the basis for further research in the direction of dielectric stresses of the circuit breakers contact gap, state of gas along the circuit breaker nozzle, as well as some simulation software improvements.

References

[1] Kapetanovic, M. 2011. *High Voltage Circuit Breakers.* Sarajevo: Elektrotehnicki fakultet.

[2] Zildzo, H., Gacanovic, R., and Matoruga, H. 2011. "Electro-Gas Model Breaking of Capacitive Currents within High Voltage SF_6 Circuit Breaker." In *Proceedings of 2011 XXIII International Symposium on Information, Communication and Automation Technologies,* 1-7.

[3] Delic, S., Beslija, D., Muratovic, M., Kim, M. H., Kapetanovic, M., and Zildzo, H. 2014. "New Approach to Breakdown Voltage Estimation after Interruption of Capacitive Currents." Presented at 2014 IEEE International Power Modulator and High Voltage Conference, Santa Fe, New Mexico, USA.

[4] Blagojevic, N. 1989. "Proracun Sastava Produkata Razlaganja Idealnih i Realnih Gasova." Sarajevo: Energoinvest-IRCE (unpublished).

[5] Mou, J., Guo, J., Jiang, X., Li, X. W., Chen, B., Xin, Z. Z., and You, Y. M. 2012. C*omputer Simulation Tool for the Design and Optimation for UHV SF_6 Circuit Breakers.* General report for CIGRÉ Conference.

[6] Ahmethodzic, A., Gajic, Z., and Kapetanovic, M. 2011. "Computer Simulation of High Voltage SF_6 Circuit Breakers: Approach to Modeling and Application Results." *IEEE Transactions on Dielectrics and Electrical Insulation* 18 (4): 1314-22.

[7] Steinbruck, H. 2014. "Institute of Fluid Mechanics and Heat Transfer." Accessed July 16, 2014. http://cdlab2.fluid.tuwien.ac.at/.

[8] Computational Fluid Dynamics Online. 2014. Accessed July 16, 2014. http://www.cfd-online.com/Wiki/Hydraulic_diameter.

Appendix

Table 1A Overview of output variables for the analyzed 420 kV circuit breaker for chosen arcing times and test duty.

Output variables from HV CB simulation	Analyzed 420 kV, 63 kA CB nozzle (L75 47.25 kA)		
Arc duration (ms)	10	15	20
Contact travel = Contact distance + Contact penetration (mm)	252.412 + 92	342.811 + 92	409.431 + 92
Nozzle inlet hydraulic diameter (mm)	100.088	100.088	100.088
Main nozzle outlet hydraulic diameter (mm)	35.0558	67.8348	67.8348
Auxiliary nozzle outlet hydraulic diameter (mm)	32.7538	32.7538	32.7538
Nozzle inlet area (m^2)	0.0204304	0.0204304	0.0204304
Main nozzle outlet area (m^2)	0.00319121	0.00402898	0.00402898
Auxiliary nozzle outlet area (m^2)	0.00084239	0.00084239	0.00084239
Static pressure at nozzle inlet (Pa)	2,155,782	2,534,408	2,647,433
Static temperature at nozzle inlet (K)	802.366	991.919	1,241.45
Specific gas density at nozzle inlet (m^3/kg)	0.0254	0.022694	0.027277
Specific heat capacity at constant volume at nozzle inlet (J/kg·K)	994.877	1,022.265	1,046.984
Specific heat capacity at constant pressure at nozzle inlet (J/kg·K)	936.731	964.848	989.912
Speed of sound at nozzle inlet (m/s)	222.723	249.08	279.024
Gas mass flow at nozzle inlet (kg/s)	10.49	11.201	10.572
Static pressure at main nozzle outlet (Pa)	599,374.75	861,570.5	1,018,623.2
Static temperature at main nozzle outlet (K)	322.374	464.194	544.431
Specific gas density at main nozzle outlet (m^3/kg)	0.028894	0.030071	0.030129
Specific heat capacity at constant volume at main nozzle outlet (J/kg·K)	731.796	861.434	908.939
Specific heat capacity at constant pressure at main nozzle outlet (J/kg·K)	654.882	799.862	849.438
Speed of sound at main nozzle outlet (m/s)	135.806	165.554	180.452
Gas mass flow at main nozzle outlet (kg/s)	9.085	9.719	9.191
Static pressure at auxiliary nozzle outlet (Pa)	609,167	609,038.75	608,226.81
Static temperature at auxiliary nozzle outlet (K)	801.704	463.792	544.154
Specific gas density at auxiliary nozzle outlet (m^3/kg)	0.075124	0.042748	0.050617
Specific heat capacity at constant volume at auxiliary nozzle outlet (J/kg·K)	992.874	857.358	905.996
Specific heat capacity at constant pressure at auxiliary nozzle outlet (J/kg·K)	935.842	798.142	848.152
Speed of sound at auxiliary nozzle outlet (m/s)	220.67	166.205	180.915
Gas mass flow at auxiliary nozzle outlet (kg/s)	1.405	1.482	1.381

Table 2A Calculated gas mass flow on the domain boundaries for the analyzed 420 kV circuit breaker at current zero.

Used simulation tool	HV CB simulation			CFD		
Arcing duration (ms)	10	15	20	10	15	20
Gas mass flow at nozzle inlet (kg/s)	10.49	11.2	10.57	6.12	6.45	6.16
Gas mass flow at main nozzle outlet (kg/s)	9.09	9.72	9.19	5.32	5.61	5.37
Gas mass flow at auxiliary nozzle outlet (kg/s)	1.41	1.48	1.381	0.76	0.84	0.796
Ratio of gas mass flow at main nozzle outlet and nozzle inlet	0.87	0.87	0.87	0.87	0.87	0.871
Ratio of gas mass flow at auxiliary nozzle outlet and nozzle inlet	0.134	0.13	0.131	0.13	0.13	0.129